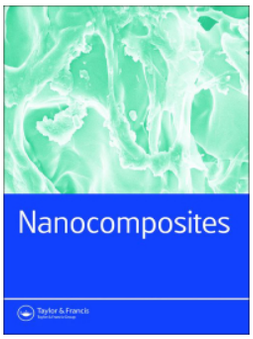

Nanocomposites

ISSN: (Print) (Online) Journal homepage: www.tandfonline.com/journals/ynan20

Effects of crystallization on micro-mechanical behavior of polyethylene nanocomposites using Raman spectroscopy

Mason Martell, Nicholas F. Mendez, Sanat Kumar, Alejandro J. Müller, George Hurd, Víctor Sebastián, David Punihaole, Rusul Mustafa, Lauren Aheran, Brian Benicewicz, Richard Ly, Huina Lin, Frederic Sansoz & Linda S. Schadler

To cite this article: Mason Martell, Nicholas F. Mendez, Sanat Kumar, Alejandro J. Müller, George Hurd, Víctor Sebastián, David Punihaole, Rusul Mustafa, Lauren Aheran, Brian Benicewicz, Richard Ly, Huina Lin, Frederic Sansoz & Linda S. Schadler (2025) Effects of crystallization on micro-mechanical behavior of polyethylene nanocomposites using Raman spectroscopy, Nanocomposites, 11:1, 68-78, DOI: 10.1080/20550324.2025.2471679

To link to this article: https://doi.org/10.1080/20550324.2025.2471679

NANOCOMPOSITES
2025, VOL. 11, NO. 1, 68–78
https://doi.org/10.1080/20550324.2025.2471679

Taylor & Francis
Taylor & Francis Group

Effects of crystallization on micro-mechanical behavior of polyethylene nanocomposites using Raman spectroscopy

Mason Martell[a], Nicholas F. Mendez[b], Sanat Kumar[b], Alejandro J. Müller[c,d], George Hurd[a], Víctor Sebastián[e,f,g,h], David Punihaole[i], Rusul Mustafa[i], Lauren Aheran[i], Brian Benicewicz[j], Richard Ly[j], Huina Lin[j], Frederic Sansoz[a] and Linda S. Schadler[a]

[a]Department of Mechanical Engineering, University of Vermont, Burlington, VT, USA; [b]Department of Chemical Engineering, Columbia University, New York, NY, USA; [c]POLYMAT and Department of Advanced Polymers and Materials: Physics, Chemistry and Technology, Faculty of Chemistry, University of the Basque Country UPV/EHU, Donostia-San Sebastián, Spain; [d]Basque Foundation for Science, IKERBASQUE, Bilbao, Spain; [e]Instituto de Nanociencia y Materiales de Aragón (INMA), CSIC-Universidad de Zaragoza, Zaragoza, Spain; [f]Department of Chemical and Environmental Engineering, Universidad de Zaragoza Campus Rio Ebro, Zaragoza, Spain; [g]Laboratorio de Microscopías Avanzadas, Universidad de Zaragoza, Zaragoza, Spain; [h]Networking Research Center on Bioengineering, Biomaterials and Nanomedicine (CIBER-BBN), Madrid, Spain; [i]Department of Chemistry, University of Vermont, Burlington, VT, USA; [j]Department of Chemistry and Biochemistry, University of South Carolina, Columbia, SC, USA

ABSTRACT

Recent work has shown that nanoparticles can be ordered in semicrystalline polymers by controlling the crystallization rate, specifically by forcing them to migrate to the amorphous regions of the lamellar morphology. Here, we study the micromechanical behavior of neat polyethylene and silica/polyethylene nanocomposites filled with 15 nm brush-modified silica in the quenched and slow-crystallized organized state. The molecular response to loading in tension was monitored with Raman spectroscopy using the peaks associated with crystalline and amorphous regions. The addition of nanofillers dramatically reduced the shift in the amorphous peaks, indicating that in addition to carrying some load, the brush-modified nanoparticles may be acting as tie molecules that restrict amorphous deformation. The higher degree of lamellar organization and the organization of the nanoparticles also impacted the crystalline peak shifts, but more subtly.

GRAPHICAL ABSTRACT

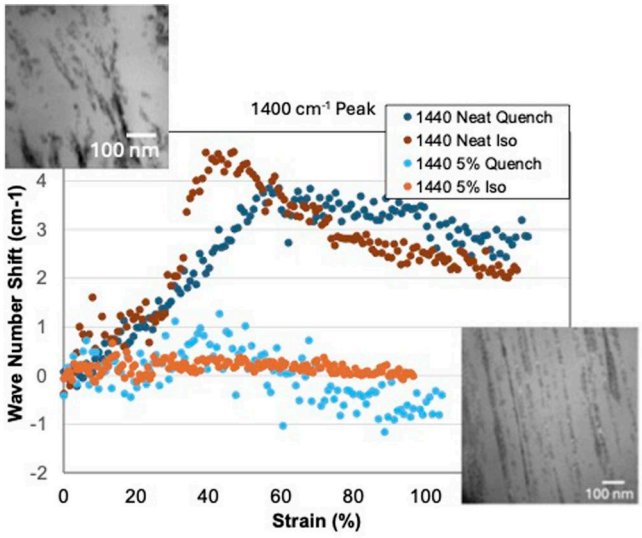

ARTICLE HISTORY

Received 18 September 2024
Accepted 20 February 2025

KEYWORDS

Polyethylene; Raman spectroscopy; crystallization; nanoparticle; grafted polymer; mechanical behavior

CONTACT Linda Schadler Linda.Schadler@uvm.edu Department of Mechanical Engineering, University of Vermont,Burlington, VT, USA

Supplemental data for this article can be accessed online at https://doi.org/10.1080/20550324.2025.2471679.

1. Introduction

Previous work has shown that during slow isothermal crystallization, growing crystalline fronts can organize NPs within amorphous regions of a semicrystalline polymer matrix [1–3]. In polyethylene oxide (where 15–50 nm silica NPs are well dispersed in the melt state), NPs will organize if crystallized at a slow enough cooling rate at molecular weights up to 100 kg/mol [4]. In polyethylene (PE), similar results have been shown in very low molecular weight PE (4k). In high molecular weight PE, polymer brushes are required to obtain good dispersion in the melt, and the organization is less perfect due to a competition between aggregation, and organization [1]. The achieved organization leads to changes in the nanocomposite mechanical and dielectric properties [1]. In this paper, we study the micromechanical behavior of neat polyethylene and nanosilica-filled polyethylene as a function of organization, particularly in the plastic region using *in-situ* Raman spectroscopy [5–8].

The ability to organize nanoparticles within the amorphous interlamellar regions of semicrystalline polymers relies on the balance between particle diffusivity and spherulitic growth rate [3,4, 9,10]. The growth rate at which these forces are balanced is described as the critical growth rate, G_c. When the growth rate, $G \gg G_c$ the NPs are engulfed by the growing crystal, whereas when $G \ll G_c$ they are rejected to the edge of the spherulites [3,4]. Maintaining a slow crystallization rate where $G \approx G_c$ allows the particles to organize within the interlamellar regions of the growing spherulites in a process referred to as crystallization-induced nanoparticle organization.

In-situ Raman spectroscopy can be used to monitor the local molecular response to macroscopic strain. It is non-destructive and the Raman peak position is sensitive to applied strain [5–8]. This relationship was first quantified in depth by Wool [5] and Wool et al. [6] for high-density, ultra-high molecular weight, ultra-drawn, extruded polyethylene films. Stress was applied parallel to the *c*-axis direction of orientation, and Raman spectra were collected in the linear-elastic region in a stepwise fashion. A linear relationship between peak position and strain was found in the elastic region.

Kida et al. [7,8] expanded on this work by tracking Raman peak location *in-situ* and for undrawn polyethylene. Incident laser light was polarized parallel to the direction of the applied load. The shift in the Raman peak, $\Delta\nu$, is negative when the corresponding molecular structure is in tension and positive in compression. They were able to correlate the Raman peak shifts with established plastic deformation mechanisms.

Figure 1 shows the Raman spectra for polyethylene with the accompanying table showing the relevant peak positions and molecular motion [5–8]. The antisymmetric and symmetric C-C stretching modes at 1063 and 1130 cm^{-1}, respectively, are sensitive to the loading of the main chain. Both peaks are representative of long trans-chains which are mostly found in crystalline structures. There is a strong peak at 1300 cm^{-1} which represents the CH_2 twisting mode for crystalline chains. There are three peaks in the 1400 cm^{-1} region, all of which represent CH_2 bending modes (1418, 1440, and 1460 cm^{-1}). The 1418 cm^{-1} band represents CH_2 bending in exclusively orthorhombic crystalline chains and was used by Kida et al. [8] to track crystalline load sharing and orthorhombic lattice position. Load in intermediate amorphous chains is tracked with the 1440 cm^{-1} band. This vibrational mode is most sensitive to interchain interactions. The band at 1460 cm^{-1} represents the CH_2 bending mode for the mobile amorphous fraction. In this work, the 1400 cm^{-1} peaks were not always distinguishable, and only the 1440 cm^{-1} peak was clearly observed and

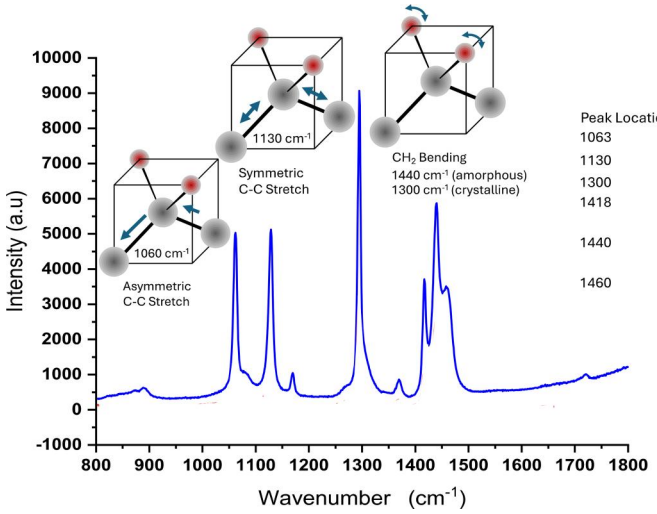

Peak Location (cm^{-1})	Mode	Phase
1063	ν_{as} (C-C)	Trans-chain
1130	ν_s (C-C)	Trans-chain
1300	ν_t (CH_2)	Crystalline
1418	δ (CH_2)	Crystalline
	ω (CH_2)	(orthorhombic)
1440	δ (CH_2)	Amorphous trans-chain
		(intermediate)
1460	δ (CH_2)	Amorphous

Figure 1. Raman spectra showing a schematic of symmetric/antisymmetric C-C stretching and CH_2 scissoring bending modes for PE with associated Raman peaks (1063, 1130, and 1440 cm^{-1}, respectively). The table labels the full set of peaks [4,6,7]. ν_{as}: anti-symmetric stretching, ν_s: symmetric stretching, ν_t: twisting, δ: bending, ω: wagging.

reported. There is an additional C-C stretching peak for amorphous chains at 1080 cm^{-1}, but it is too weak experimentally to effectively follow.

Tensile plastic deformation of PE is characterized by local deformation in both the crystalline and amorphous phases. While the details are still under discussion in the recent literature, local cavitation, lamellar kinking and fragmentation, accompanied by shear deformation in the amorphous layers (Figure 2), as well as interlamellar separation, are the mechanisms operating in the plastic region. Recent work [11,12] has shown that modification of the amorphous regions by swelling with small molecules can impact the local deformation by limiting cavitation. While this does not alter the other operating mechanism during deformation, cavitation enables slip localization and lamellar fragmentation at lower strains.

In the elastic region, Kida et al. [7,8] shows that the crystalline peaks do not shift indicating that the elastic stress is carried in the amorphous regions. They note a small upward peak shift (compression) just after yield, followed by a negative shift once drawing begins, suggesting a transition from compressive to tensile loading in the crystalline regions as Figure 2 suggests. The amorphous peaks were found to show a very small compressive shift in the elastic region, followed by a larger positive shift (compression) after the first yield point and a negative shift (tension) once drawing begins. This indicates that there is a local lateral compressive stress in the amorphous regions due to lamellar micro buckling and the morphology preventing lateral shrinkage. As lamellar orientation and stretching occur, the stress in the amorphous regions is released. In this work, we study the impact of the nanoparticles on this local response in order to understand the impact of nanoparticles on the micromechanical response of the composite.

2. Materials and methods

2.1. Materials

15 nm silica nanoparticles from Nissan Chemical were chemically modified using poly(cyclooctene-*b*-succinic anhydride) (p(CO-*b*-SA)) and *n*-octadecyltrimethoxysilane (C18-Si$(OCH_3)_3$) to create a bimodal population of grafted ligands (C-18 and a polymer chain). The grafted poly(cyclooctent) (PCO) chains were further reduced using *p*-toluenesulfonyl hydrazide to form linear polyethylene (PE) chains. The number average molecular weight and graft density of grafted PE chains were characterized to be 84 kg/mol and 0.136 chains/nm^2, respectively. The particles were solution blended with a 50 kg/mol matrix to a loading of 33.4 wt% [13].

Prior work has shown that dispersion is enhanced if the matrix molecular weight is below that of a low-density brush [14]. The 50k molecular weight, M_w, PE with a polydispersity of less than 1.5, however, was too brittle to use in high-strain tensile experiments. To balance dispersion and ductility, a 100k M_w PE matrix was blended with the 50k M_w PE to create a model bidisperse matrix. This matrix was mixed in a Haake MiniCTW twin-screw compounder at 145 °C using an equal parts blend of 50k and 100k M_w PE. The screw rpm was ramped up from 20 rpm to 75 rpm over 5 min to maintain 0.5Nm torque on the screws. The neat PE blend was then extruded and allowed to cool to room temperature.

2.2. Polymer nanocomposite (PNC) production

For this study, the PNC was diluted through melt mixing to create a 50:50 50k and 100k M_w PE blend with 5 wt% core loading. This material was mixed in a twin screw extruder at 150 °C for 5 min. The screw rpm was ramped from 20 rpm to 60 rpm to maintain torque at 0.5 Nm. The material was extruded and

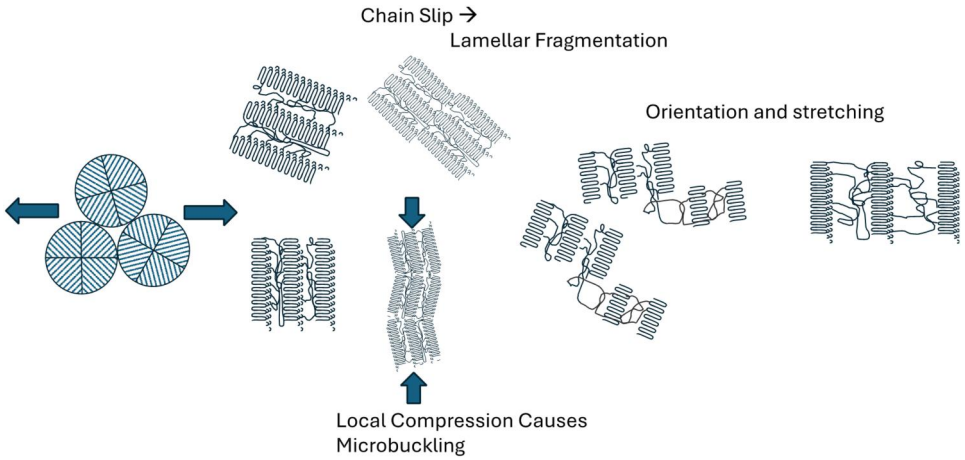

Figure 2. Schematic representation of deformation behavior of HDPE crystals under uniaxial load including the compression created for lamella with a perpendicular orientation, the microbuckling and chain slippage that occurs after yield, and ultimately the lamellar fragmentation and drawing.

allowed to cool to room temperature. Core silica loading was confirmed to be 5 wt% through thermogravimetric analysis.

2.3. Compression molding

Blended PE samples were compression molded in a small hot press using a custom stainless steel tensile mold based on a modified ASTM D638 Type V standard at 0.5 mm thickness. The hot press was preheated to 160 °C and the sample pre-loaded into the mold. The material was then melted and pressed into the mold and held at temperature. Quenched samples were held at 160 °C for 5 min under pressure, after which the hot press was quickly air-cooled to room temperature with fans. Samples that would later undergo isothermal crystallization were held at 160 °C for 2 min and then quenched to limit degradation.

2.4. Isothermal crystallization

In order to determine the appropriate isothermal crystallization temperature to allow for nanoparticle organization (e.g. slower than Gc), melting temperatures and crystallization enthalpies were measured in a Netzsch DSC 214 Polyma. A range of temperatures a few degrees higher than the onset of crystallization were chosen for each sample and tested to identify which provided sufficiently slow crystallization over a ~12-hour isothermal heating cycle to allow for particle organization. It was determined that for neat PE, 115 °C and for the PNC 117 °C achieved that result.

2.5. Small angle X-ray scattering (SAXS)

SAXS was performed on a SAXSLAB instrument using a Cu K α source with a photon energy of 8.04 keV ($\lambda = 1.54$ Å). A moving Pilatus 300k detector was used with a variable sample-to-detector distance that covers a q range of 0.004–0.2 $Å^{-1}$. The resulting 2D detector images were processed and integrated into a 1D intensity profile $I(q)$ using SAXSLAB's saxsgui software.

2.6. In-situ *Raman experimental setup*

A similar method to that used by Kida et al. [7,8] for tensile testing of samples with *in-situ* Raman spectroscopy was used (Figure 3). A Kammrath and Weiss Tensile/Compression stage equipped with a 500-N load cell and flat grips was integrated into a custom Raman spectrometer by mounting the stage to a plate perpendicular to the spectroscopy table [15]. This allowed the laser light to be perpendicular to the sample in the tensile stage. Raman bands were excited with a 532 nm Torus laser polarized parallel to the direction of tensile loading. The beam was attenuated with an ND wheel to lower the power to 24mW at the sample and focused through an infinity-corrected Olympus Ach 10x/0.25 NA long working distance objective. Each sample's gauge thickness and width were measured with calipers before testing, while the gauge length was standardized by the mold dimensions.

The custom Raman setup is described in detail by Mustafa et al. [15]. Briefly, scattered light was directed into an Acton SpectraPro 2500i spectrometer controlled with LightField software from Teledyne Princeton Instruments (TPI). The light was dispersed in the spectrometer using a 600 gr/mm ruled grating and imaged with a PIXIS 400B CCD camera from TPI. The nominal resolution of the spectrometer is 1.7 cm^{-1} at 532 nm using a 600 gr/mm grating. Raman spectra and tensile data were collected simultaneously, with a 3 s spectral acquisition time and an elongation rate of 3 μm/s.

On initial setup, the laser light was focused with the objective's micrometer stage. The sample was left in the setup with the laser on to allow fluorescence to burn off. The spectra were observed and the objective re-focused every 30 min until the intensity of the spectra no longer decreased. At this point, the tensile test and Raman data acquisition were started in parallel. Since the tensile stage has

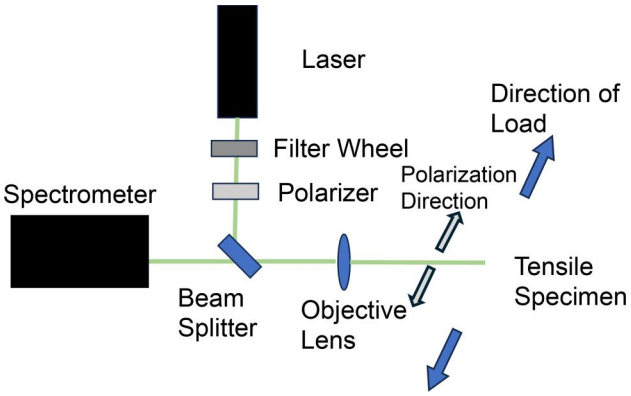

Figure 3. Schematic representing the experimental setup for *in-situ* Raman spectroscopy of a specimen under tensile load.

limited elongation capacity, the tests were stopped before the sample reached 150% strain.

2.7. Data analysis

Raman spectral data collection parameters were set using the software LightField. Spectra often had raised and non-linear baselines due to background noise. A GUI was created in MATLAB to fit baselines within spectral windows to improve subsequent fitting. The program fit a baseline for each spectrum and subtracted it from the spectrum to normalize the data. Baseline-subtracted spectra were exported to a second MATLAB program to fit the data [16]. This program averaged spectra based on user input and fit peaks using a sum of pseudo-Voigt functions, outputting peak locations and intensities (Figure 4).

3. Results and discussion

3.1. DSC and SAXS analysis

Results from DSC are shown in Table 1. Percent crystallinity (X_c) for composite samples was normalized by the weight fraction of filler and all X_c values were calculated using an equilibrium melting enthalpy of $\Delta H_m = 296\,\mathrm{J/g}$ [17]. No significant changes in crystallinity were observed across all samples (including neat polymers vs. nanocomposites, and across cooling protocols).

Lorentz corrected SAXS data is shown in Figure 5 with Lorentz corrected intensity, Iq^2, as a function of scattering vector, q. The long period (L_p) of lamellar stacks within polymer spherulites, defined as the width of a crystalline lamella plus the width of an interlamellar amorphous region, was calculated from SAXS curves ($L_p = 2\pi/q$). In both neat and PNC samples isothermal crystallization increased the long period. The long period of neat quenched and isothermal samples was estimated to be ~26.5 nm and ~33 nm, respectively. PNC quenched and isothermal samples show a long period of ~26.2 nm and ~38.4 nm, respectively.

The upturn of the scattering data at low q values from the PNC samples crystallized isothermally indicates the presence of structures larger than the long period, likely resulting from NP agglomerates. The peaks present in the PNC isothermal sample show that despite the aggregation evidenced from the upturn at low q, there is the interlamellar organization of some of the particles. This ordering also gives rise to the first reflection peak at ~17.9 nm. While there may be some overlapping contribution from the scattering of the polymer long period, the electron density difference between silica and PE will be dominant over the contrast between the amorphous and crystalline PE electron density. These results are further supported by TEM images (Figure 6). The isothermally crystallized neat polymer has larger and more organized lamellae. The quenched PNC has small agglomerates, and the isothermally crystallized PNC is a mixture of small but elongated agglomerates and regions where the nanoparticles seem to be organized between the lamellar regions.

3.2. Tensile testing with in-situ Raman spectroscopy

Figure 7 shows a comparative plot for the engineering stress-strain curves of the four samples and the

Table 1. DSC results for neat PE and PNC samples.

Sample	T_m (°C)	T_c (°C)	ΔH_m (J/g)	X_c (%)
Neat quench	136.4	111.4	203	69
Neat isothermal	140.7	109.1	210	71
PNC quench	138.6	109.3	186	67
PNC isothermal	139.7	108.9	194	69

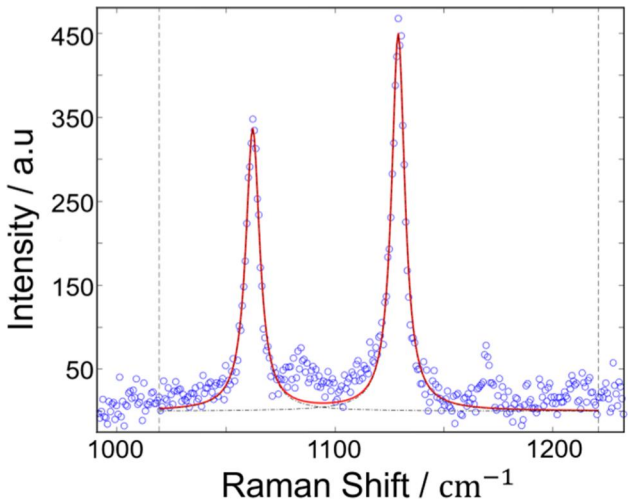

Figure 4. Representative example spectrum fit for 1063 and 1130 cm^{-1} peaks. Blue circles are raw spectrometer data, red lines are the curve fit and baseline, and dashed black lines are estimated peaks. Overall, the standard errors of the center frequencies extracted from the peak fits ranged between 0.1 and 0.5 cm^{-1}.

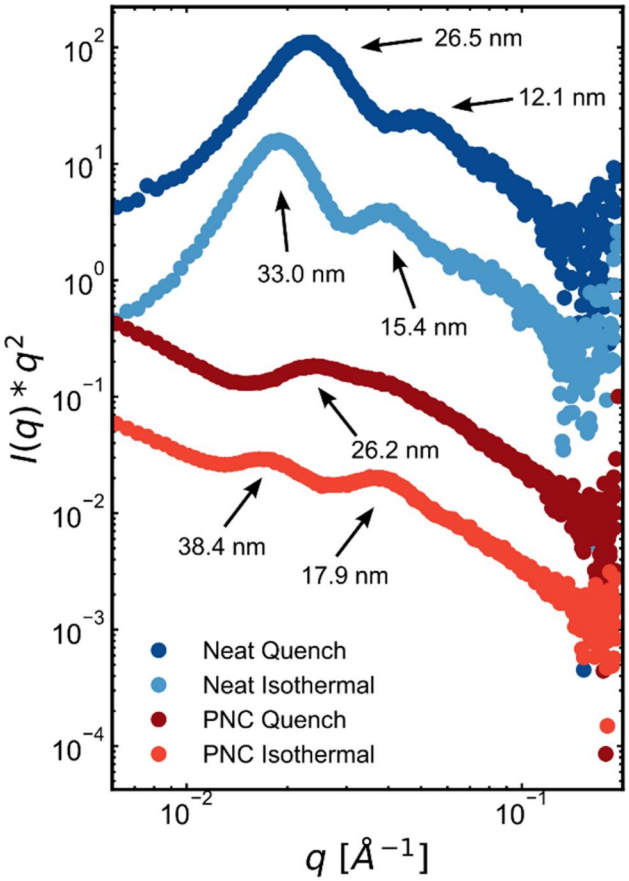

Figure 5. 1D SAXS traces of neat PE and PNC samples for both quenched and isothermal crystallization processes.

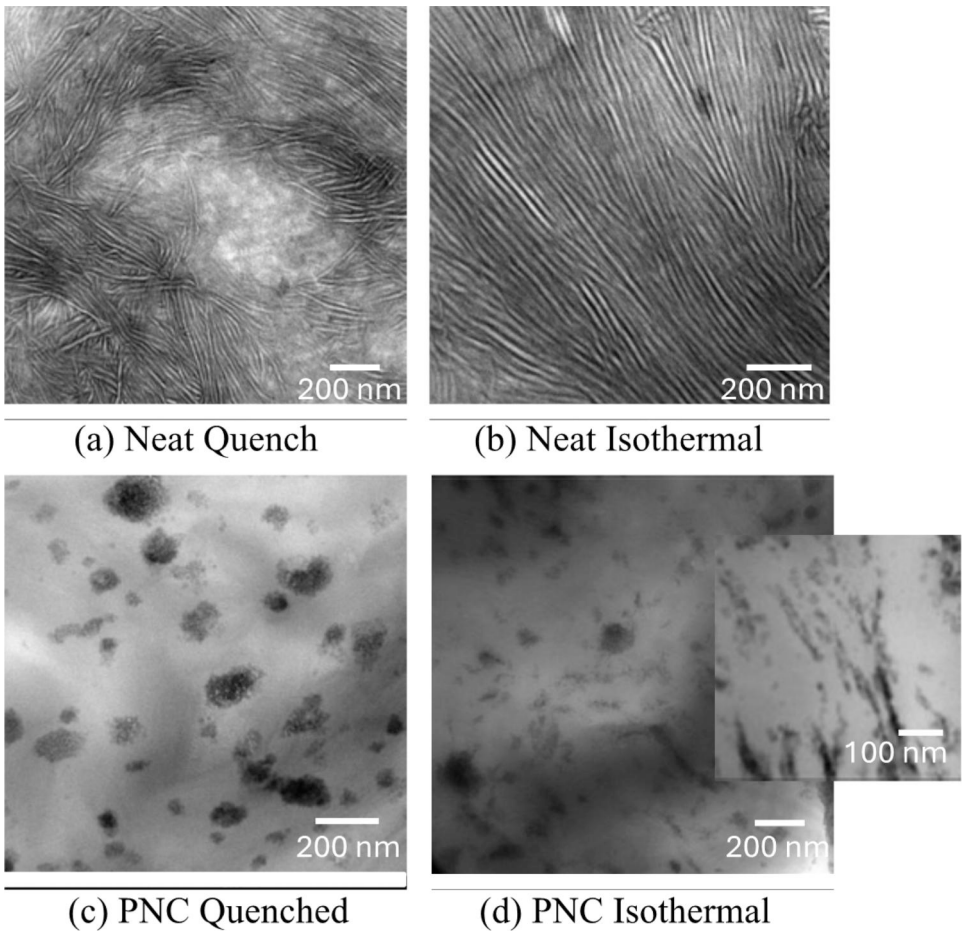

Figure 6. TEM micrographs of the untested samples (a) neat polyethylene quenched (stained with RuO_4), (b) neat polyethylene isothermally crystallized for 8 h at 115 °C (stained with RuO_4), (c) 5 wt% silica filled polyethylene quenched (no staining), and (d) 5 wt% silica filled polyethylene isothermally crystallized for 8 h at 114 °C (no staining).

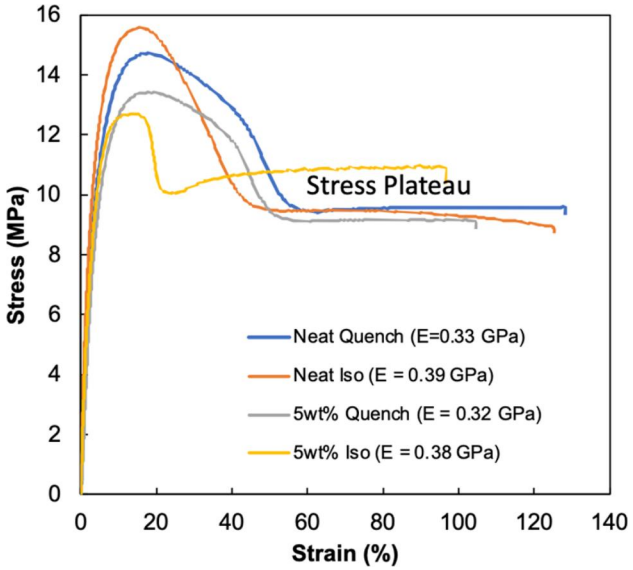

Figure 7. Example tensile test results for all samples, including the yield point and the Plateau. Young's modulus (E) is in the legend.

Young's moduli for each. Young's modulus was calculated as the slope of the stress-strain curve in the linear-elastic region. Isothermal samples have a higher modulus than their neat counterparts. Given the similar crystallinity, this may be due to the more organized lamellae. The PNCs show very similar moduli to the neat polymer which is not surprising given the small particle loading (5 wt%). The strain at yield, defined by the maximum in the engineering stress-strain curve, is about the same for the neat samples and the quenched PNC ~20%. The isothermally crystallized PNC has a maximum in stress at ~15% strain. The quenched samples reach a stress plateau at ~60% strain while the isothermally crystallized PE reaches that stress plateau at ~40% strain. The isothermally crystallized PNC plateaus at about 20% strain. The lower strain at yield and for the stress plateau is likely the impact of a defect, as the second sample showed a higher first yield point, but failed soon after. Thus, the isothermally crystallized samples are clearly more prone to failure. This does not, however, impact the overall conclusions from the work.

Raman peak locations were measured *in situ* during the uniaxial stretching of samples. The crystalline CH_2 twisting peak at 1300 cm^{-1} had a strong intensity in all samples tested. Peaks for PNC samples contain more noise than neat PE due to a high level of observed fluorescence. Shifts of 1063, 1130, 1300, and 1440 cm^{-1} peaks for quenched and isothermally crystallized neat PE are shown in Figure 8.

In all samples, the crystalline peaks do not shift in the elastic region. In the neat samples, the 1130 cm^{-1} peak is relatively stable. The 1300 cm^{-1} peak (CH_2 crystalline) shows a negative shift (tension) between the yield and the stress plateau and then is relatively stable. The 1063 cm^{-1} peak (asymmetric C-C stretch) decreases constantly in the plastic region in the quenched sample. In the isothermally crystallized sample, there is an increase just after yield, followed by a rapid decrease, and then a linear slope consistent with that of the quenched sample. The increase in peak position suggests early compression on the lamella consistent with other work, followed by stress release and then a constant increase in stress/strain carried by the crystalline regions during drawing [8].

The 1440 cm^{-1} amorphous peak is strongly influenced by the surrounding peaks, but all are associated with the amorphous region. In both neat samples, the 1400 cm^{-1} peak shifts immediately into compression in the elastic region. This compressive force is a result of the rigid crystalline lamella resisting shrinkage perpendicular to the direction of load during necking. The shift is steeper in the elastic region for the quenched sample suggesting that the lamellar disorganization due to quenching leads to earlier strain in the amorphous region. Both samples show a maximum in the 1440 cm^{-1} peak at about the point where the stress plateau begins, followed by a release of the stress. The increase in the 1440 cm^{-1} is larger in the isothermal sample (and the stress plateau begins at a lower strain – 40%). The subsequent decrease is larger, though both samples plateau at around 2 cm^{-1} shift. The rapid change of the 1440 cm^{-1} peak in the isothermally crystallized sample after yield indicates that the amorphous regions are rapidly loaded, and then as the lamella begins to break up and orient during drawing, this strain is released.

For the isothermally crystallized sample, both 1400 cm^{-1} and 1063 cm^{-1} peak shifts less than in

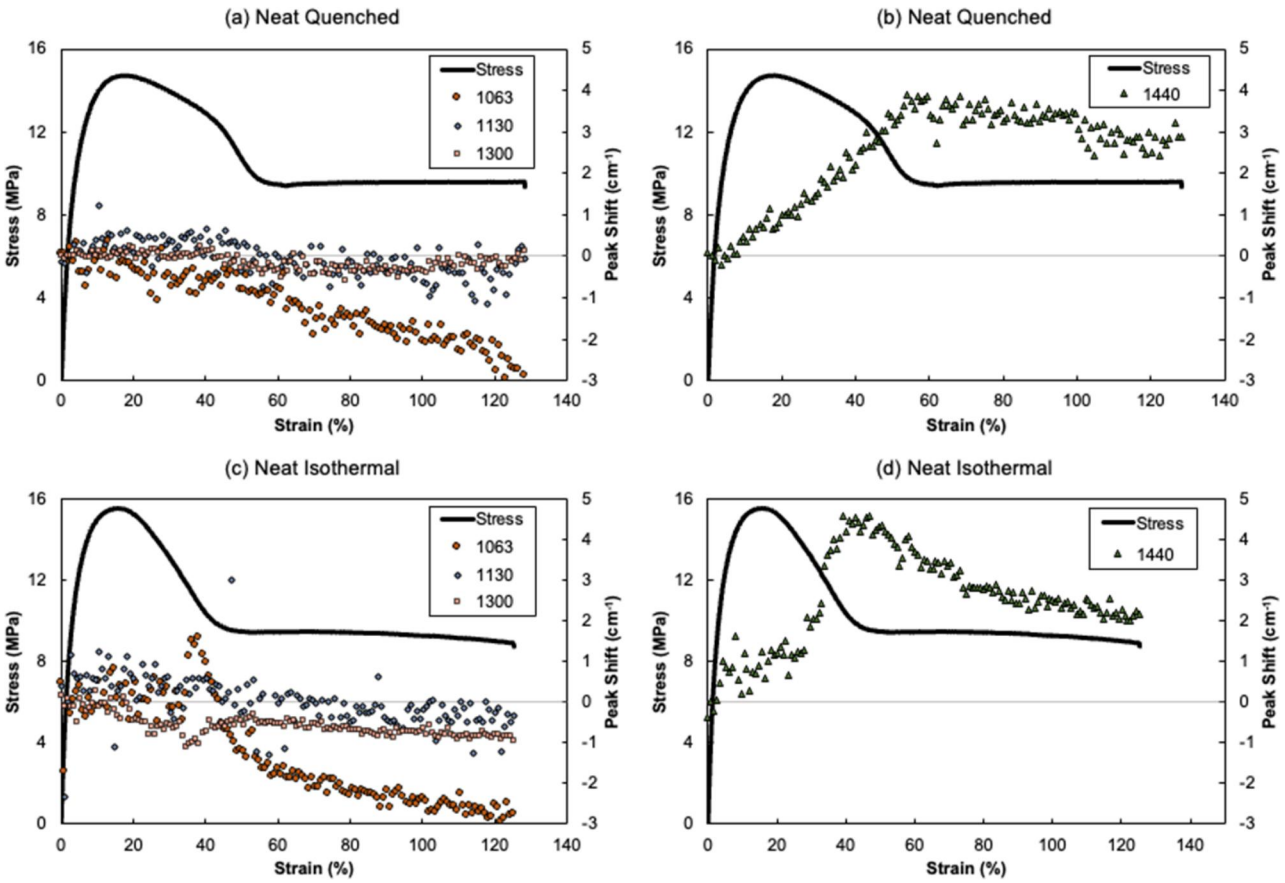

Figure 8. Stress-strain curve and Raman peak shift for quenched (a,b) and isothermally crystallized (c,d) neat PE. Plots compare shifts for crystalline (1063, 1130, and 1300 cm^{-1}) and amorphous (1440 cm^{-1}) peaks.

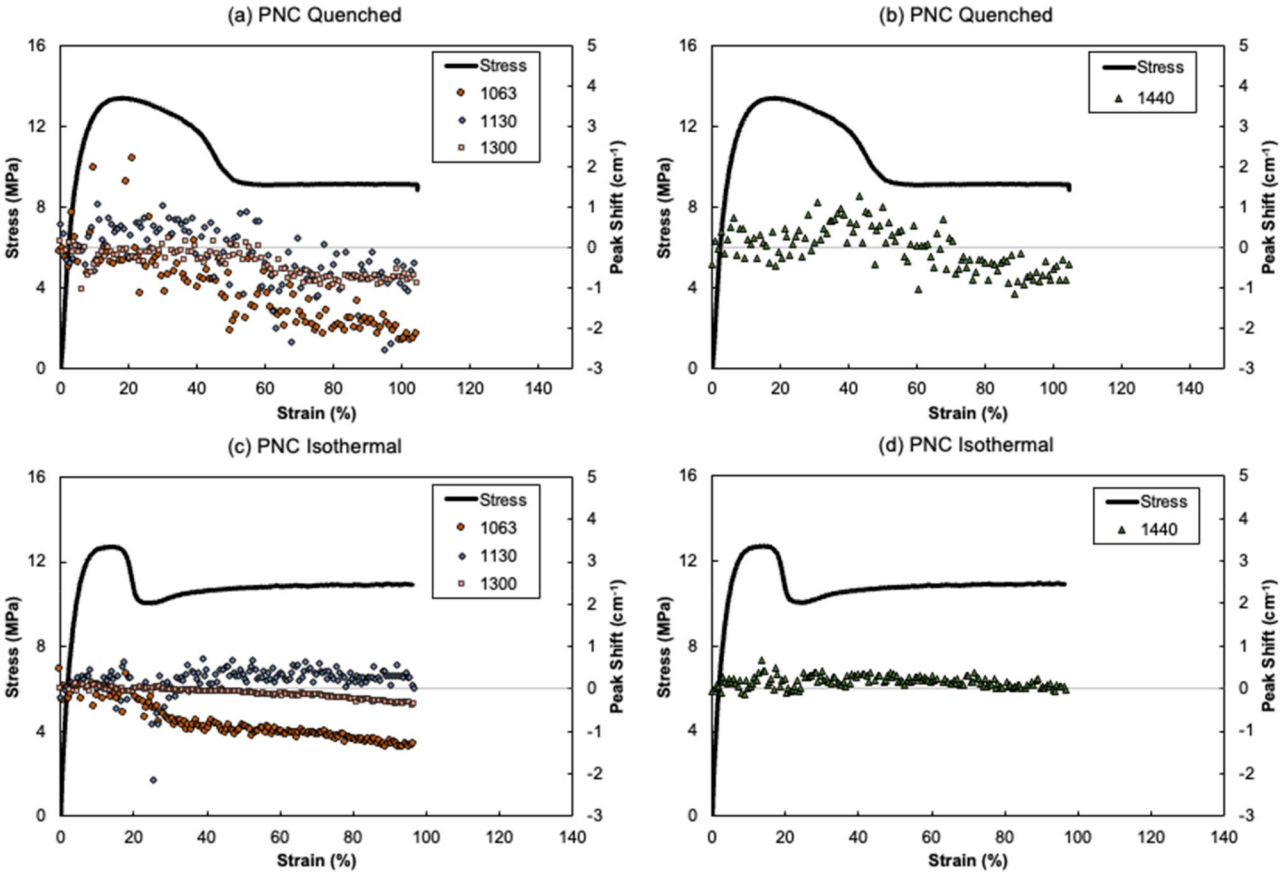

Figure 9. Stress-strain curve and Raman peak shift for quenched (a,b) and isothermally crystallized (c,d) PNC. Plots compare shifts for crystalline (1063, 1130, and 1300 cm^{-1}) and amorphous (1440 cm^{-1}) peaks.

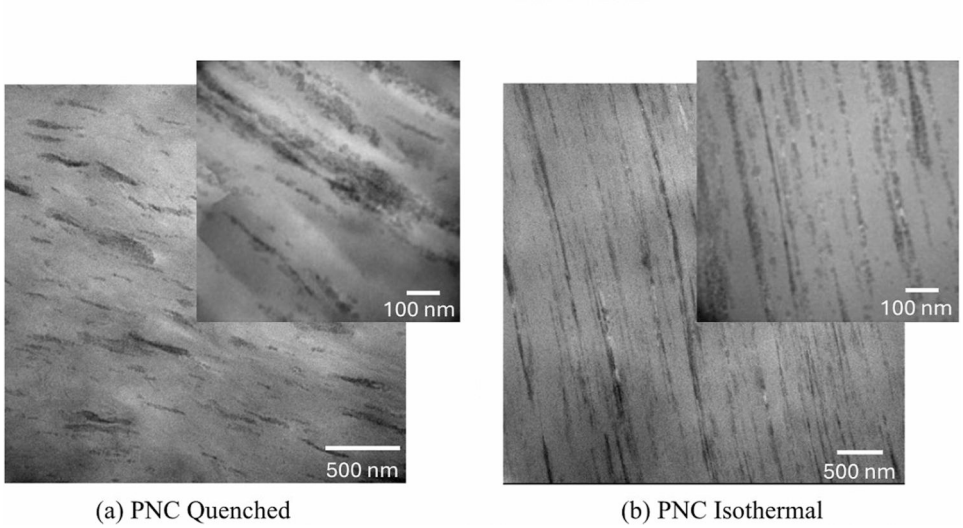

Figure 10. TEM micrographs (unstained) of the fully drawn PNC samples (a) quenched, (b) isothermally crystallized at 114 °C.

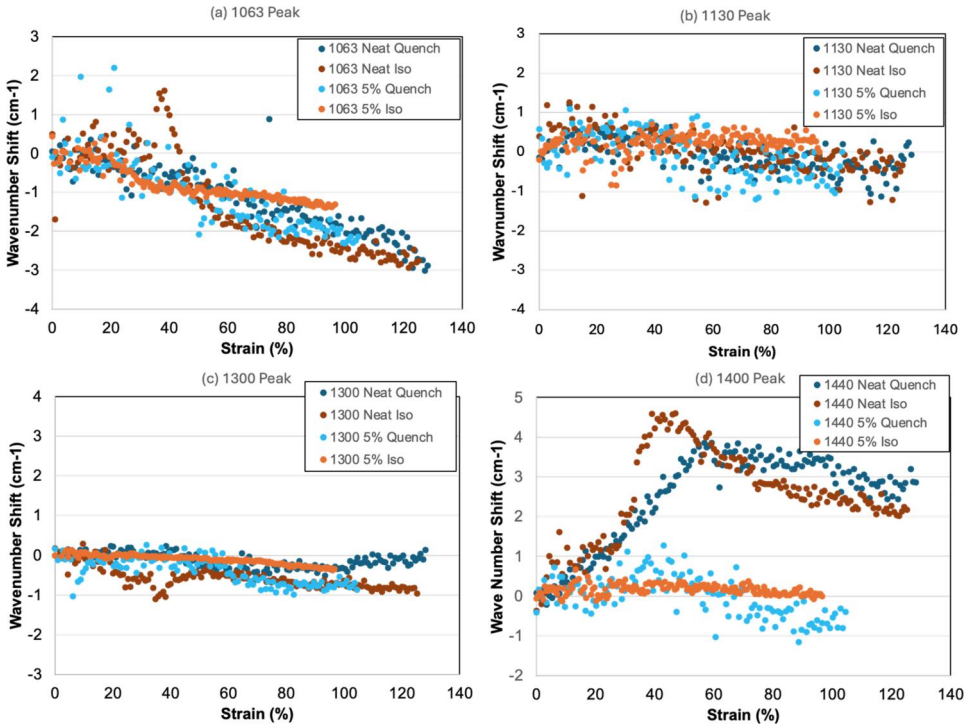

Figure 11. Comparison of the Raman peak position across all 4 samples. (a) 1063 cm^{-1} peak, (b) 1130^{-1} peak, (c) 1300 cm^{-1} peak, and (d) 1440 cm^{-1} peak.

the quenched sample at low strain. After yield, but before the stress plateau, both peaks have a rapid positive peak shift. This indicates that the amorphous and asymmetric crystalline peaks experience compression at yield, which is subsequently released (and eventually becomes tensile in the 1063 cm^{-1} peak) during drawing.

Figure 9 shows the results for the PNC. The biggest difference between the neat and PNC samples is that the 1440 cm^{-1} peak does not shift significantly for the PNC samples. In the quenched sample it shows a small compressive shift and then a tensile shift, greatly attenuated compared to the neat samples, and in the isothermally crystallized sample, no shift is observed. This suggests that the amorphous regions are not carrying significant stress or strain in these samples. The nanoparticles have polymer chain ligands that are designed to entangle with the matrix. Thus, with this entanglement between the chains grafted to the particles and the matrix chains, it is likely that the nanoparticles are acting to reinforce the amorphous region and due to the stiffness of the particles, they limit deformation in the amorphous regions. Since the quenched sample has larger agglomerates that are more widely spaced apart, this limits their impact, and thus, more of a shift is observed than in the isothermally crystallized sample.

The crystalline peaks for the PNC quenched sample are very similar to the neat sample. This indicates that the larger agglomerates have not impacted the crystalline deformation significantly but are carrying the strain (instead of the amorphous regions). For the PNC isothermal sample, the crystalline peak shifts are about half that of the quenched sample. The combined results suggest that the semi-organized and elongated particle clusters are carrying a significant amount of the load, reducing the load carried by the polymer.

Evidence of the deformation in the agglomerates of the quenched PNC and in the semi-organized nanoparticles in the isothermally crystallized PNC is clear in the TEM of the fully drawn samples (Figure 10). These samples were cut parallel to the loading direction. They illustrate the better dispersion and more organized structure of the isothermally crystallized samples and the resulting chain-like organization of the nanofillers. This results in greater load-carrying ability in the plastic region.

Figure 11 compares each peak across each of the 4 samples. Within the resolution of the Raman spectrometer, there are no significant differences for the 1130 cm^{-1} and 1300 cm^{-1} peaks. It is clear, however, that for the 1063 cm^{-1} peak, the isothermally crystallized PNC has a significantly lower slope in the drawing region (~0.02 wavenumbers/percent strain vs. ~0.01 wavenumbers/percent strain). In addition, the amorphous peak (1440 cm^{-1}) shifts significantly less for the PNC samples.

4. Summary and conclusions

The DSC results show that the crystallinity in all samples is very similar (Table 1). Thus, any changes observed are due to changes in the morphology. For example, a larger long period is observed in isothermal samples ($D \approx$ 33.0 nm) versus quenched ($D \approx$ 26.5 nm). This same increase in a long period is observed in the PNCs. The low loading (5 wt%) would not be expected to significantly change the long period even if the NPs were well-organized in the amorphous regions. In the composite samples, scattering peaks are influenced by the presence of NPs. The upturn at very low q values of PNC samples indicates the presence of NP agglomerates. TEM micrographs support this but also show that in the isothermally crystallized samples, there is some alignment of nanoparticles within the lamellar morphology.

Kida et al. [8] reported that the crystalline structure in PE lamellae remains stable until yield when the orthorhombic crystals begin to disorder and orient into the direction of load. As a neck forms after the first yield point, the disordered crystals quickly orient, and inter-crystal spacing increases. In the present work, this is seen as the 1440 cm^{-1} transitions from a positive to negative direction of shift as the amorphous molecules transfer strain to the crystals which are orienting in the direction of load.

In the composites, the presence of the brush-modified silica nanoparticles significantly reduces the strain carried by the amorphous regions. This is surprising given the loading and the size of the nanoparticles. One hypothesis is that the brushes on the NPs entangle with the matrix chains and thus serve as significant tie molecules that transfer the load between crystals and limit the strain in the amorphous region. Support for this ansatz is that the particles stay connected during drawing, indicating that they are entangled with each other in some way and, thus, likely also with the matrix.

Acknowledgements

The authors are grateful for the support from the U.S. Department of Energy, Office of Science, Office of Basic Energy Sciences, Division of Material Sciences and Engineering under Award DE-SC0020847 (LS), DE-SC0018135 (BC), DE-SC0018111 (SK) and DE-SC0020054 (FS). NFM acknowledges funding from the NSF GRFP through grant DGE-2036197.

Disclosure statement

No potential conflict of interest was reported by the authors.

ORCID

Nicholas F. Mendez http://orcid.org/0000-0002-2080-3041
Sanat Kumar http://orcid.org/0000-0002-6690-2221
Víctor Sebastián http://orcid.org/0000-0002-6873-5244
David Punihaole http://orcid.org/0000-0002-4637-9672
Rusul Mustafa http://orcid.org/0000-0003-3175-2427
Brian Benicewicz http://orcid.org/0000-0003-4130-1232
Huina Lin http://orcid.org/0000-0002-7379-5313
Frederic Sansoz http://orcid.org/0000-0002-2782-1832
Linda S. Schadler http://orcid.org/0000-0002-6406-5247

References

1. Ning X, Jimenez AM, Pribyl J, et al. Nanoparticle organization by growing polyethylene crystal fronts. ACS Macro Lett. 2019;8(10):1341–1346. doi: 10.1021/acsmacrolett.9b00619.
2. Bornani K, Mendez NF, Altorbaq AS, et al. *In situ* atomic force microscopy tracking of nanoparticle migration in semicrystalline polymers. ACS Macro Lett. 2022;11(6):818–824. doi: 10.1021/acsmacrolett.1c00778.
3. Zhao D, Gimenez-Pinto V, Jimenez AM, et al. Tunable multiscale nanoparticle ordering by polymer crystallization. ACS Cent Sci. 2017;3(7):751–758. doi: 10.1021/acscentsci.7b00157.

4. Mendez NF, Altorbaq AS, Müller AJ, et al. Organizing nanoparticles in semicrystalline polymers by modifying particle diffusivity. ACS Macro Lett. 2022;11(7):882–888. doi: 10.1021/acsmacrolett.2c00287.
5. Wool RP. Mechanisms of frequency shifting in the infrared spectrum of stressed polymer. J Polym Sci Polym Phys Ed. 1975;13(9):1795–1808. doi: 10.1002/pol.1975.180130912.
6. Wool RP, Bretzlaff RS, Li BY, et al. Infrared and Raman spectroscopy of stressed polyethylene. J Polym Sci B Polym Phys. 1986;24(5):1039–1066. doi: 10.1002/polb.1986.090240508.
7. Kida T, Tanaka R, Shiono T, et al. Direct observation of the effect of a high-molecular-weight component on the deformation behavior of polyethylene solids using the Rheo-Raman spectroscopic technique. Macromolecules. 2023;56(8):3073–3082. doi: 10.1021/acs.macromol.3c00197.
8. Kida T, Hiejima Y, Nitta K. Raman spectroscopic study of high-density polyethylene during tensile deformation. Int J Exp Spectroscopic Tech. 2016;1(1):1–6. doi: 10.35840/2631-505X/8501.
9. Mendez NF, Dhara D, Zhang Q, et al. Nanoparticle diffusion in miscible polymer nanocomposite melts. Macromolecules. 2023;56(12):4658–4668. doi: 10.1021/acs.macromol.3c00490.
10. Keith HD, Padden FJ. Spherulitic crystallization from the Melt. I. Fractionation and impurity segregation and their influence on crystalline morphology. J Appl Phys. 1964;35(4):1270–1285. doi: 10.1063/1.1713606.
11. Bartczak Z, Vozniak A. Deformation instabilities and cavitation in plastic deformation of semicrystalline polyethylene. Macromolecules. 2024;57(14):6474–6491. doi: 10.1021/acs.macromol.4c00642.
12. Oleinik E. Plasticity of semicrystalline flexible-chain polymers at the microscopic and mesoscopic levels. Polymer Sci C. 2003;45:17–117.
13. Pribyl J, Benicewicz B, Bell M, et al. Polyethylene grafted silica nanoparticles prepared via surface-initiated ROMP. ACS Macro Lett. 2019;8(3):228–232. doi: 10.1021/acsmacrolett.8b00956.
14. Akcora P, Liu H, Kumar SK, et al. Anisotropic self-assembly of spherical polymer-grafted nanoparticles. Nat Mater. 2009;8(4):354–359. doi: 10.1038/nmat2404.
15. Mustafa R, Fitian M, Hamilton NB, et al. Molecular insights into the binding of linear polyethylenimines and single-stranded DNA using Raman spectroscopy: a quantitative approach. J Phys Chem B. 2022;126(42):8404–8414. doi: 10.1021/acs.jpcb.2c04939.
16. Bower DI, Maddams WF. The vibrational spectroscopy of polymers. Cambridge University Press; 1989. doi: 10.1017/CBO9780511623189.
17. Sertchook H, Elimelech H, Makarov C, et al. Composite particles of polyethylene @ silica. J Am Chem Soc. 2007;129(1):98–108. doi: 10.1021/ja0653167.